Estimating the effect of cooling rate on the acquisition of magnetic remanence

Estimating the effect of cooling rate on the acquisition of magnetic remanence

Lesleis Nagy[1], **Wyn Williams**[2], **Lisa Tauxe**[1]

[1]Scripps Institution of Oceanography, UC San Diego
[2]School of GeoSciences, University of Edinburgh

Key Points:

- Previous efforts to estimate cooling rate effects result in different corrections.
- Our model agrees well with the model of Halgedahl et al. (1980).
- The source code of our model is available for verification and further development.

Corresponding author: Wyn Williams, wyn.williams@ed.ac.uk

This article has been accepted for publication and undergone full peer review but has not been through the copyediting, typesetting, pagination and proofreading process, which may lead to differences between this version and the Version of Record. Please cite this article as doi: 10.1029/2021GL095284.

Abstract

The effect of cooling rate on the magnetization of rocks must be accounted for when estimating ancient magnetic field strengths. Calculating this effect is not trivial, even for uniformly magnetized grains. Here, we present an open-source package to compute the behaviour of uniaxial single-domain grains for different temperature and magnetic fields. We revisit the problem of thermal remanence acquisition as a function of cooling rate and find that our predictions are broadly in agreement with those of Halgedahl et al. (1980) but differ significantly from those of Dodson and McClelland-Brown (1980). We also find that remanence acquisition curves correspond well with recent experimental observations. Cooling rate corrections made using our model are at the upper limit suggested by Halgedahl et al. (1980) but can reduce slightly for larger (single-domain) grains, very slow cooling rates of the original thermal remanence and large field strengths.

Plain Language Summary

The Earth's magnetic field is one of the most fundamental features of our planet, with some studies indicating that that it has been active as early as the Hadean (Tarduno et al., 2020). Knowing how the ancient field strength changes through time provides valuable information about significant geological events in our planet's past, such as when its inner core formed. The ancient field is recorded in rocks, which act as natural storage devices. However, the speed with which a rock cools in the presence of the field greatly affects the recorded signal. This means that estimates of the Earth's ancient field must be 'cooling rate corrected'. Our results show that one of the earlier approaches to calculating theoretical corrections will underestimate the ancient field whereas the other is very good. Our work also matches well with recent experimental data; and additionally, we provide a free and open-source implementation of our software that may be used to investigate the effect of in-field cooling for many different field and temperature scenarios.

1 Introduction

Accurately recovering the strength of the Earth's ancient magnetic field (paleointensity) is a critical part of understanding our planet's history. For example, such observations inform us about how the solid inner-core evolved through time, and of particular current interest, when it formed. The rate at which a sample cooled in the presence of an ancient field is an important factor in accurately determining palaeointensity. This is especially the case when attempting to reconstruct historical field intensities from samples that have cooled over long periods of time. For example, Selkin et al. (2000) established that the field was present by 2.7 Ga, and some have argued for an even earlier onset (Tarduno et al., 2010). At the time, this was taken to mean that the inner core was present since inner core nucleation is a powerful source of energy for the geodynamo. However, the work of Pozzo et al. (2012) called into question the energy source and the hunt began for the timing of inner core formation (Driscoll, 2016). Recent efforts have pointed to the Ediacaran (Bono et al., 2019) and the estimate of a much younger inner core forming just $\sim$0.57 Ga ago, prior to which a much weaker paleomagnetic field might be expected. All but the most rapidly cooled paleointensities (which approach the laboratory cooling rate) require estimates of the behavior of magnetic remanence as a function of cooling rate which can lead to overestimates of field strength by up to 50% or underestimates by more than 10%, depending on domain state (see recent review by Santos and Tauxe (2019) and references therein).

Currently there is no complete theory of the precise mechanism for thermally activated recording in non-single domain (SD) grains. There is, however, a firm theoretical foundation for the simpler case of ensembles of SD grains. Using Néel's theory (Néel, 1949), Dodson and McClelland-Brown (1980) examined the effect of slow cooling on the

blocking temperature of ensembles of SD particles. A concurrent effort was undertaken by Halgedahl et al. (1980), who modelled the effect of cooling rate on the acquisition of paleointensity in several different cooling scenarios (regimes). Unfortunately there is a mismatch in predicted thermal remanent magnetization (TRM) between these twin efforts. (Santos & Tauxe, 2019).

In this study, we revisit the single domain model of remanence acquisition from Néel's theory of elongate single-domain grains, referred to as Stoner-Wohlfarth grains after Stoner and Wohlfarth (1948). We take advantage of advances in numerical computation capability since the early 1980s and provide a fast and publicly available code, written in C++, that calculates TRM gained as a function of cooling in an external field. This code uses the Boost multiprecision library (Boost, 2021) to avoid possible numerical issues that arise when calculating the fractional alignments of non-interacting grains that make up our model. We then examine a number of cooling and field regimes and produce a new set of cooling rate correction curves and find that our results agree well with the cooling rate curves provided by Halgedahl et al. (1980) for the majority of the size elongation and field scenarios in this study.

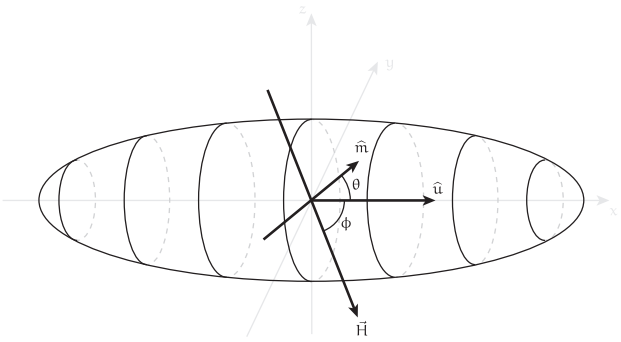

Figure 1. The Stoner-Wohlfarth model of magnetization assumes an ellipsoidal grain oriented along the vector $\widehat{u}$. The applied field $\vec{H}$ (of strength H) and the magnetization $\widehat{m}$ makes angles ϕ and θ (respectively) with $\widehat{u}$. The model assumes that the magnetization will rotate within the $\widehat{u} - \vec{H}$ plane, and so for an arbitrary angle θ we can always recover a three dimensional magnetization vector.

2 Methods

2.1 The Stoner-Wohlfarth model

The Stoner-Wohlfarth model (Stoner & Wohlfarth, 1948) describes the energy barriers that a simple uniformly magnetized uniaxial ferromagnetic grain, with ellipsoidal geometry, must overcome to change its magnetic state in the presence of an externally applied field $\vec{H}$. The external field makes an angle ϕ with the grain's axis of elongation $\widehat{u}$ as shown in Figure 1. The magnetic state is the angle θ between the unit magnetization vector $\widehat{m}$ and the grain axis $\widehat{u}$. An expression for the magnetic energy of the system envisioned originally by Néel (1949) is given by Dunlop and Özdemir (2001) [pp. 207] and can be written as

$$E(\theta, T) = C_1(T)\sin^2\theta - C_2(T)\cos\theta - C_3(T)\sin\theta, \tag{1}$$

with the temperature dependent constants $C_1(T)$, $C_2(T)$ and $C_3(T)$ given by

$$C_1(T) = \frac{1}{2}\left(N_b - N_a\right) v\mu_0 M_\mathrm{s}\left(T\right)^2, \tag{2}$$

$$C_2(T) = Hv\mu_0 \cos\phi M_\mathrm{s}\left(T\right), \tag{3}$$

$$C_3(T) = Hv\mu_0 \sin\phi M_\mathrm{s}\left(T\right). \tag{4}$$

$M_\mathrm{s}(T)$ is the saturation magnetization at temperature T, μ_0 is the permeability of free space and the particle volume is v. The strength of an externally applied field is H and its direction is given by ϕ, as described previously, with θ the direction of magnetization.

The demagnetizing factors of a prolate ellipsoid, with aspect ratio m, are defined in Cullity and Graham (2011) [pp. 54], with N_a and N_b corresponding to the demagnetizing factors along the long and short axes respectively as shown in Equations 5 & 6

$$N_a = \frac{1}{m^2-1}\left(\frac{m}{\sqrt{m^2-1}}\log\left(m+\sqrt{m^2-1}\right)-1\right), \tag{5}$$

$$N_b = \frac{1-N_a}{2}. \tag{6}$$

It should be noted that in this study we quote elongation as a percentage as opposed to aspect ratio where elongation is defined by $m = (\text{elongation} + 100)/100$. This means that an aspect ratio of 1.3 corresponds to an elongation of 30%.

In order to find the critical points for the energy of a Stoner-Wohlfarth particle we look for the values of θ where the first derivative of (1) with respect to θ is zero, doing this gives

$$\frac{\partial E\left(\theta,T\right)}{\partial\theta} = 2C_1(T)\cos\theta\sin\theta + C_2(T)\sin\theta - C_3(T)\cos\theta = 0. \tag{7}$$

There is no general analytical solution for Equation 7 except for the special cases when $\phi = 0$ and $\phi = \pi$. However we can numerically find the zeros by making the substitution $\theta = i\log(x)$ where $i = \sqrt{-1}$. This then transforms Equation 7 from a trigonometric one into the polynomial

$$-1 - \left(\frac{C_2(T) - iC_3(T)}{C_1(T)}\right)x + \left(\frac{C_2(T) + iC_3(T)}{C_1(T)}\right)x^3 + x^4 = 0, \tag{8}$$

from which we can form the upper Hessenberg matrix (Press et al., 2007) [pp. 469]

$$\mathcal{H} = \begin{pmatrix} -\left(\frac{C_2(T)+iC_3(T)}{C_1(T)}\right) & 0 & \left(\frac{C_2(T)-iC_3(T)}{C_1(T)}\right) & 1 \\ 1 & 0 & 0 & 0 \\ 0 & 1 & 0 & 0 \\ 0 & 0 & 1 & 0 \end{pmatrix}. \tag{9}$$

The eigenvalues of $\mathcal{H}$ are the zeros of the polynomial version (Equation 8), and are found using the Eigen linear algebra library (Guennebaud et al., 2010). Then we calculate the critical θ-values, denoted θ_k, by using our original transform $\theta = i\log\left(x\right)$. This results in $\theta_k \in [-\pi, \pi]$, with each θ_k solving Equation 7. Any θ_k values that have non-zero imaginary parts are discarded as these do not represent real magnetization directions.

2.2 Thermal theory of remanence

We briefly review the thermal theory of single domain remanence with particular reference to the implementation details in our C++ code. We are interested in both a 'cooled remanence' which solves the thermal equations with the assumption that grain assemblages spend only a finite amount of time at a given temperature and the 'equilibrium remanence' which is the theoretical limit for which a grain has spent an infinite amount of time at each temperature step.

2.2.1 Cooled remanence

Once the critical values of Equation 1 are found, we can evaluate whether they correspond to energy minimum/maximum states by taking the second derivative of Equation 7, which results in

$$\frac{d^2E(\theta)}{d\theta^2} = 2C_1\cos(2\theta) + C_2\cos(\theta - \phi). \tag{10}$$

When Equation 10 is positive for any critical value θ_k, then we have found a local energy minimum (LEM) state and the critical value is denoted $\theta_{k,\min}$. Likewise θ_k values that make Equation 10 negative correspond to local energy maxima and are denoted $\theta_{k,\max}$. The energy barrier for a two state system is then given by

$$\Delta E_{k,j} = \min\left(E(\theta_{k,\max}) - E(\theta_{j,\min})\right). \tag{11}$$

We take the energy barrier as the transition energy between any two LEM states, $\theta_{k,\min}$ and $\theta_{j,\min}$, as this represents the physical path that the magnetization would take when transitioning between any two LEM states. The isothermal transition rate matrix (Fabian & Shcherbakov, 2018), denoted P, may now be formed from the above energy barrier calculations by assuming that a grain population (given by the vector $\vec{\rho}_t$ described below), has experienced the same field and temperature conditions for a given time Δt

$$P(\Delta t) = \exp\left[\begin{pmatrix} \frac{1}{\tau_0}e^{\frac{\Delta E_{1,1}}{Tk_B}} & -\frac{1}{\tau_0}e^{\frac{\Delta E_{1,2}}{Tk_B}} \\ -\frac{1}{\tau_0}e^{\frac{\Delta E_{2,1}}{Tk_B}} & \frac{1}{\tau_0}e^{\frac{\Delta E_{2,2}}{Tk_B}} \end{pmatrix}\Delta t\right], \tag{12}$$

where T is the temperature of the grain in Kelvin, $1/\tau_0 = 10^{10}$ Hz is the attempt frequency (Dunlop & Özdemir, 2001), k_B is Boltzmann's constant and 'exp' is the matrix exponential function (see Appendix A1). Equation 12 may then be used to calculate an updated grain population $\vec{\rho}_{t+\Delta t}$ according to

$$\vec{\rho}_{t+\Delta t} = P(\Delta t)\vec{\rho}_t. \tag{13}$$

For a *monodispersion* of grains, which is a population of grains with a single size and shape shape we define a "population vector". Each element of the population vector represents the fraction of grains that occupy a particular magnetization state. This means that $\rho_{k,t+\Delta t}$ must sum to unity and that each element indexed by a specific LEM state k must be consistent with its predecessor $\rho_{k,t-\Delta t}$. The normalized magnetization is then given by

$$\vec{m}_{k,t} = \rho_{k,t}\cdot\vec{m}(\theta_{k,\min}), \tag{14}$$

where $\vec{m}(\theta_{k,\min})$ represents the conversion of the magnetization LEM angle, that solves the Stoner-Wohlfarth equations described above, back to a three dimensional vector (see Appendix A2).

2.2.2 Equilibrium remanence

To estimate the effect of cooling rate, we need to also estimate the equilibrium TRM, which is defined as the magnetization reached when an ensemble (population) of particles have experienced a given field and temperature for an infinite amount of time. The equilibrium population vector $\vec{\rho}_{\text{eq}}$ components are given by Dunlop and Özdemir (2001) [pp. 213] as

$$\vec{m}_{\text{eq},t} = \frac{\sum_k \vec{m}\left(\theta_{k,\min}\right)\exp\left(\frac{-E(\theta_{k,\min})}{Tk_B}\right)}{\sum_k \exp\left(\frac{-E(\theta_{k,\min})}{Tk_B}\right)}. \tag{15}$$

2.3 Cooling models

The effect of cooling was calculated for a number of different cooling regimes with temperatures given by classical Newtonian cooling

$$T(t) = (T_0 - T_{\text{amb}}) \exp\left(\frac{t_0 - t}{t_0 - t_1} \log\left(\frac{T_1 - T_{\text{amb}}}{T_0 - T_{\text{amb}}}\right)\right). \tag{16}$$

Here (t_0, T_0) is an initial time-temperature pair which we take to be $t_0 = 0$ seconds and T_0 is the Curie temperature of magnetite in degrees centigrade. The other known time-temperature point along the cooling curve, (t_1, T_1), is taken to be $T_1 = 15.15°\text{C}$ (since in the Newtonian cooling model the ambient temperature is an asymptote) and for t_1 - the time taken to reach T_1 - we use $t_1 = 6{\times}10^e$ seconds (with $e \in 1, 2, \ldots, 15$) to give a range of 'rapid' to 'slow' cooling rates. Finally the ambient temperature, T_{amb}, is 15°C.

3 Results and discussion

The results in Figure 2 and Figure 3 show that the magnitude of the TRM as a function of applied field in 'rapid' and 'slow' cooling regimes. The main difference between Figures 2 and 3 is that the applied field for Figure 2 is directed along the grain axis $\widehat{u} = \langle 1, 0, 0\rangle$ whereas the field in Figure 3 is directed along $\langle 1, 1, 1\rangle$, forming an angle of 54.7° with respect to the grain axis.

In both figures, it can be observed that TRM increases as a function of grain size, expressed as equivalent spherical volume diameter (ESVD), and remains approximately linear as a function of applied field. In all cases, the TRM acquired increases from rapid to slow cooling times as is evident from the way the solid lines fan out from left to right as the cooling times become longer. We expect this is because for slow-cooling, the grain has more opportunity to equilibrate with the external field, allowing a stronger magnetization to be acquired. It may also be observed that TRM drops (the solid lines fan out less) as the particles become more elongate. In order to explain this effect, it should be noted that, upon cooling, the earlier a TRM acquisition curve departs from its equilibrium behaviour, *i.e.* its blocking temperature, the smaller its room temperature remanent magnetization will be. For highly elongate grains, the rapid increase of energy barriers upon cooling results in a higher blocking temperature and so lower TRM as can be observed in Figures 2 and 3.

Energy barriers to domain switching in Stoner-Wohlfarth particles for fields parallel to the grain axis are in general higher than at other angles. For small fields similar to the Earth's field, the grain's magetization will always lie along its elongation axis and so the difference between the two possible states is higher in the field-parallel case as opposed to some other angle. This means that TRM acquisition is more efficient when the field is applied parallel to the elongation axis, as in Figure 2 when compared to the case when the field is applied at an angle (Figure 3). In addition to TRM efficiency being a function of cooling rate, the curvature of equilibrium (dashed) lines is also greater for grains with the field directed parallel to the grain axis (Figure 2) as opposed to grains with the external field directed at an angle to the grain axis (Figure 3). For example, the 80 nm dashed line in Figure 2 reaches its saturation value at ∼100 μT, whereas the same line in Figure 3 reaches the saturation value at the much higher field of ∼175 μT.

Figure 4 shows the results of our modeling along with the predictions of Halgedahl et al. (1980) (dashed black line) and Dodson and McClelland-Brown (1980) (dotted black line) along with experimental data from Santos and Tauxe (2019) and other authors (detailed in the caption of Figure 4). Our numerical calculations are for a collection of grains with *no fabric*, which is a monodispersion of grains over a random distribution of directions (with respect to applied field). The majority of the grain size and elongations correspond well with the predictions of Halgedahl et al. (1980). The most noticeable excep-

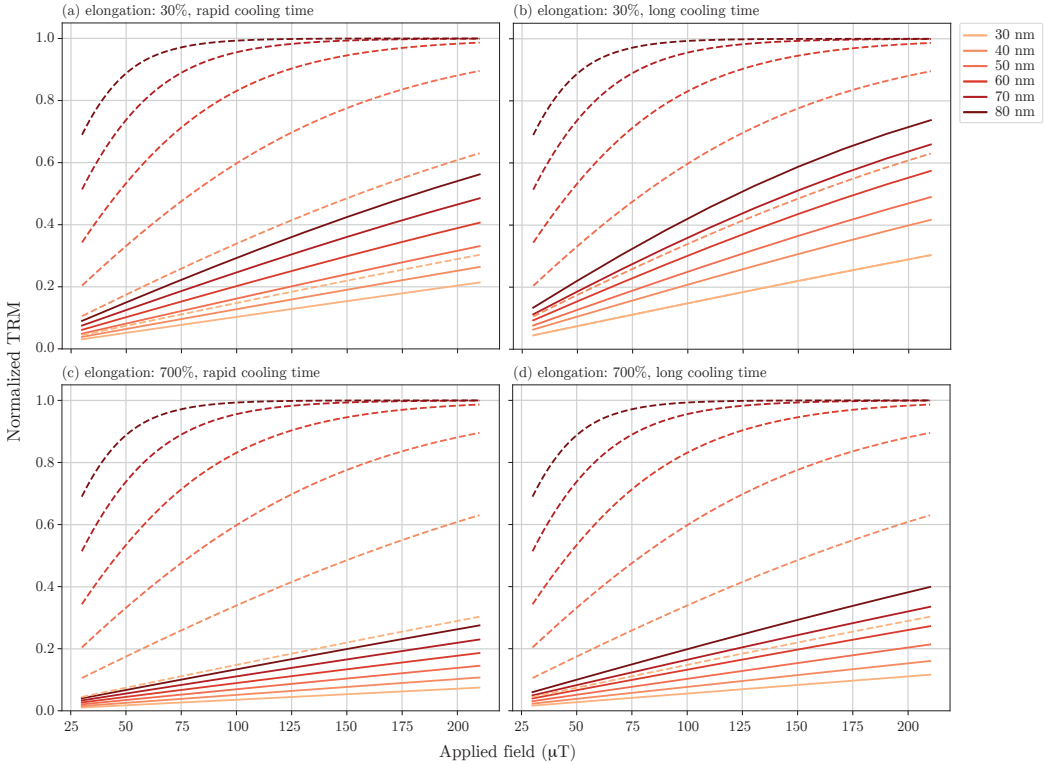

Figure 2. TRM acquisition versus applied field for cooling from the Curie Temperature (580°C) to 15.15°C as a function of grain size (ESVD) and elongation for 'rapid' ($t_1 = 6{\times}10^3$ s) and 'slow' ($t_1 = 6{\times}10^{15}$ s) cooling regimes. TRM has a value of 1.0 when all particles are aligned with the field direction. Field strengths range from 30 μT to 210 μT and are aligned parallel to the grain elongation axis $\widehat{u}$. Solid lines show TRM acquired through cooling, whereas the dashed lines show equilibrium TRM (infinite cooling time).

tion being the 30 nm 30% elongate grain (light blue line) which is border-line superparamagnetic since its volume and elongation are relatively small.

Figure 5 shows TRM acquisition curves for the complete time range for a study that goes well beyond that seen in Figure 4 with an assumed laboratory cooling time of 1000 seconds to a maximum cooling time of 190 Ma. A population of grains with a *strong fabric* (a monodispersion of grains that are all aligned with the applied field) are shown along with a set of predictions for high field strength of 210 μT. We see in Figures 5a and 5b that the spread of TRM acquisition for slow cooling is relatively small in weak fields. This is not the case for stronger fields shown in Figure 5c and 5d where there is a much greater spread. This illustrates that, in weak fields at least, elongation and grain size have little effect on TRM acquisition. It should also be noted that the highly elongate grains (red) show only relatively minor variations in all field regimes. TRM acquisition is affected by grain size, though much less so in elongate grains. This is most clearly seen in the strong field regimes in Figures 5c and 5d with both the parallel field and intermediate field showing that for slow cooling, the TRM recorded decreases as a function of grain size (we see the darker lines taking on shallower gradients). It may also be observed that in the larger grains under strong field conditions, there is a slight curvature. This is again most apparent in the 30% elongate grains, indeed the 30 nm 30% elongate grain (lightest blue) plateaus for slow cooling. As observed previously, this grain size is

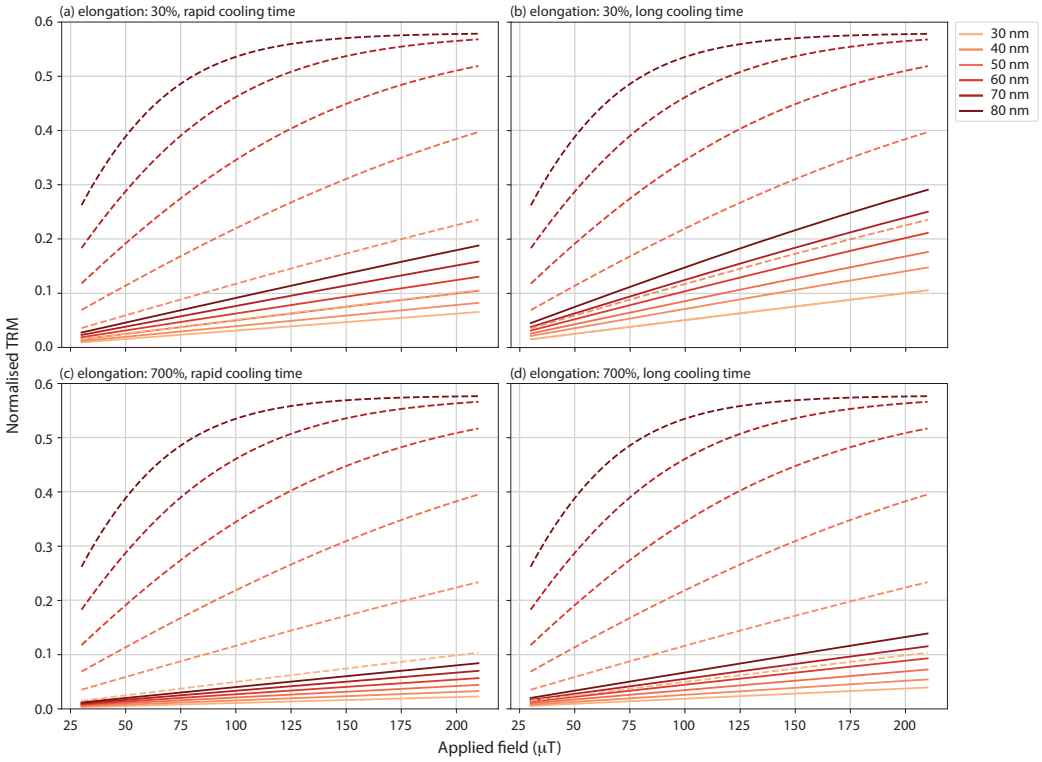

Figure 3. Same as Figure 2, but fields applied at an angle of 54.7° to the grain elongation axis $\widehat{u}$.

just on the cusp of being superparamagnetic and at a particular cooling rate the 'cooled' TRM acquisition curve achieves equilibrium. The threshold for superparamagnetic behavior is when the magnetization reaches equilibrium with the external field over the time span of observation. In the case of the 30 nm 30% elongate grain, the relaxation time is short enough when cooled slowly, for its thermal-magnetic behaviour to achieve equilibrium, meeting the definition of superparamagnetism. In principle all cooling rate curves should eventually plateau, if the cooling rate is slow enough (see Dodson and McClelland-Brown (1980) Figures 1 and 2). A final observation is that grains with strong fabric and no fabric show small differences. These differences are a drop in the ratio of TRM gained since the gradient of each line becomes very slightly shallower from strong fabric to no fabric; and an increase in the TRM ratio gained when the grain hits its equilibrium behaviour (lightest blue line). The shallower gradient is due to the fact that in simulated monodispersions with no fabric, there are many grains that have smaller energy barriers since the field is at an angle to the axis of elongation. The light blue line plateaus later (with higher ratio of TRM) for the same reason and so the cooling effect is reduced. This effect can also be seen by comparing the plateau between the weak field and the strong field in samples between the same fabric (*i.e.* between Figures 5a & 5b, and Figures 5c & 5d) since in stronger fields grains hit their equilibrium behaviour sooner.

4 Conclusions

In this study we have presented a model for calculating the TRM acquisition as a function of field and cooling rate and have found good correspondence with experimental data for single domain grains. Of the previous published models we find that our results are very close to the predictions of Halgedahl et al. (1980) Our model also demon-

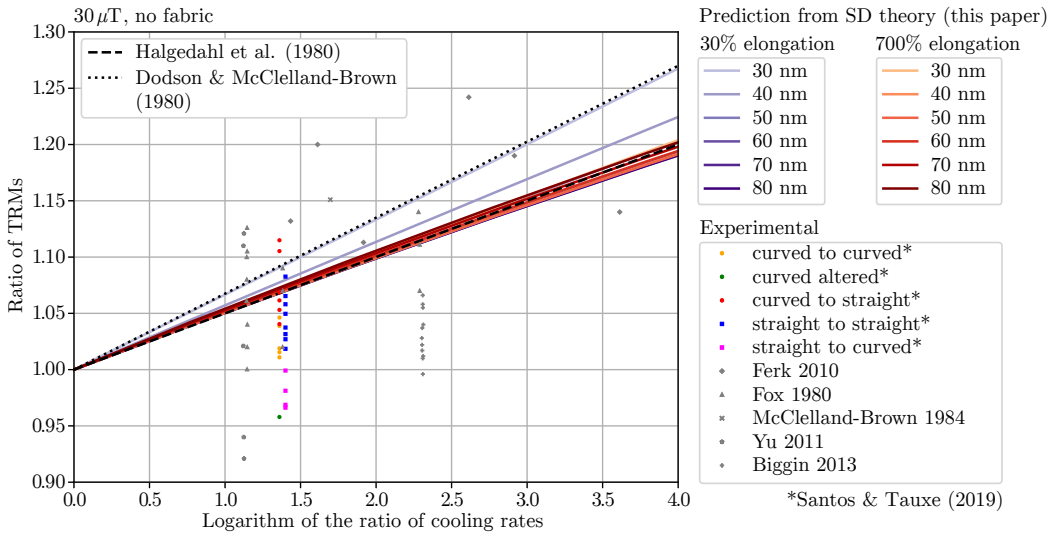

Figure 4. Acquired TRM versus cooling rate, plotted against theoretical models of Halgedahl et al. (1980) (dashed black line), and Dodson and McClelland-Brown (1980) (dotted black line). Experimental data from Santos and Tauxe (2019) (asterisks). Additional data are from Fox and Aitken (1980), McClelland-Brown (1984), Leonhardt et al. (2006), Ferk et al. (2010), Yu (2011), Biggin et al. (2013). Theoretical predictions are for 30 μT applied fields for an assemblage that that has no fabric. The two color schemes used represent grains with 30% elongation in shades of blue and 700% elongation in shades of red; with the lighter shades correspond to smaller grains by volume (ESVD).

strates subtle variations in recording as a function of grain size and shape, however we also show that there is relatively little variation in remanence acquisition as a function of field strength and direction (at least for weak fields like the Earth's).

The source code for the model that we have presented is freely available at `https://github.com/Lesleis-Nagy/sd-cooling` (version 1.0.1 was used in this study). Currently it based on simple Stoner-Wohlfarth modeling described, however the thermal theory of remanence described in this study is also applicable to grains with much more complicated magnetizations and switching mechanisms. For more realistic grains we require micromagnetic modelling such as MERRILL (Ó Conbhuí et al., 2018) to compute the energy barriers involved in switching from one magnetization state to another. We view this as the way forward to build accurate and realistic models of paleomagnetic samples.

Appendix A Additional details

A1 Exponential of a matrix

Computing the exponential of an arbitrary matrix is non-trivial and several approaches are possible. One numerically stable and general technique involves the use of Padé approximations (Press et al., 2007) and this is the solution taken in Eigen (Guennebaud et al., 2010) but is currently incompatible with the Boost multi-precision library (Boost, 2021). In this study we use eigenvalue decomposition to calculate the matrix exponential. Let $A = RDR^{-1}$, where R is the matrix of eigenvectors and D is the diagonal matrix of eigenvalues, then

$$\exp(A) = R\exp(D)R^{-1}, \tag{A1}$$

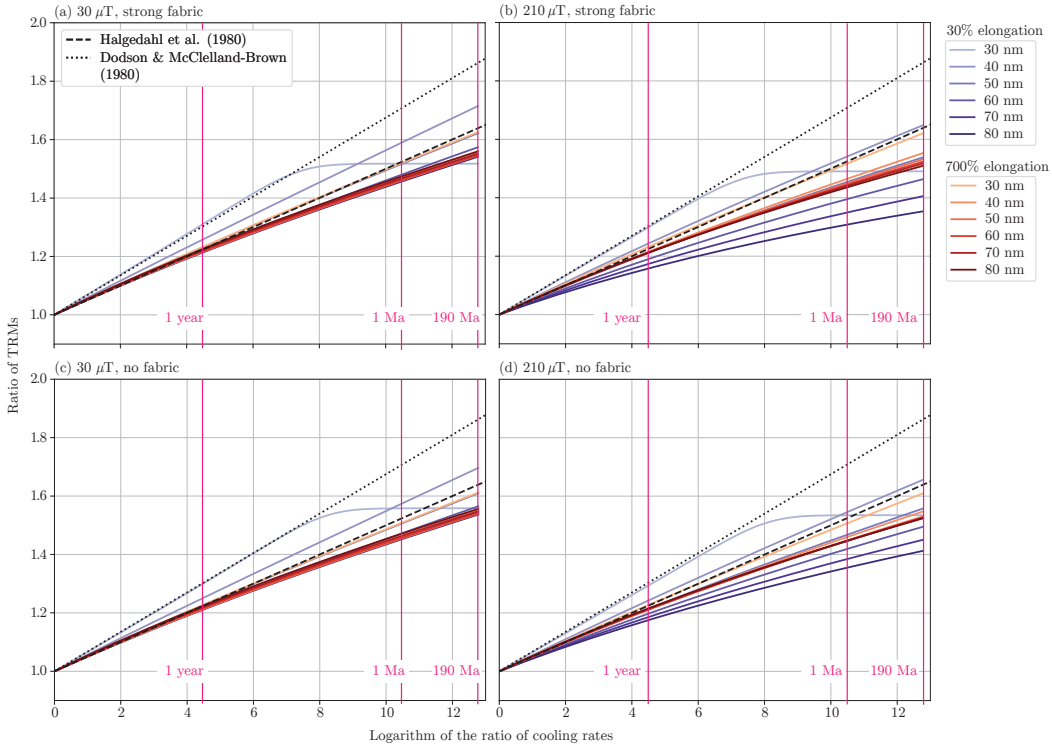

Figure 5. Acquired TRM versus cooling rate plotted against theoretical models of Halgedahl et al. (1980) (dashed black line), and Dodson and McClelland-Brown (1980)(dotted black line) for the complete time range in this study with (a) an assemblage in weak field with strong fabric, (b) an assemblage in a strong field with strong fabric, (c) an assemblage in weak field with no fabric and (d) an assemblage in strong field with no fabric. The colour scheme is the same as in Figure 4. Cooling rates are calculated with respect to a laboratory reference cooling time of one thousand seconds. In order to apply a cooling rate correction, simply divide the sample age (in seconds) by the laboratory reference time and take the base ten logarithm, after that the ratio of remaining TRM can be read off from the graph (depending on the grain characterization of the sample).

and $\exp(D)$ is just the simple exponential of all the entries of D on the diagonal and zero everywhere else.

A2 Conversion of a magnetization angle to a vector

In order to convert LEM state solutions, $\theta_{k,\min}$, of the Stoner-Wohlfarth equations to three dimensional vectors, we assume that the applied field $\vec{H}$ and the grain axis $\widehat{u}$ in Figure 1 form a plane in which $\widehat{u}$ will rotate by $\theta_{k,\min}$ to give the magnetization. The vector

$$\widehat{r} = \frac{\vec{H} \times \widehat{u}}{\left|\vec{H} \times \widehat{u}\right|} \tag{A2}$$

then forms the axis of rotation and

$$\vec{m}(\theta_{i,\min}) = \mathcal{R}\left(\widehat{r}, \theta_{i,\min}\right) \widehat{u}, \tag{A3}$$

with $\mathcal{R}\left(\widehat{r},\theta_{i,\min}\right)$ the the 3×3 rotation matrix given by

$$\mathcal{R}\left(\widehat{r},\theta\right)_{j,j} = \cos\theta + r_j^2\left(1-\cos\theta\right) \tag{A4}$$

on the diagonal and

$$\mathcal{R}\left(\widehat{r},\theta\right)_{x,y} = r_x r_y\left(1-\cos\theta\right) - r_z\sin\theta \tag{A5}$$
$$\mathcal{R}\left(\widehat{r},\theta\right)_{y,x} = r_x r_y\left(1-\cos\theta\right) + r_z\sin\theta \tag{A6}$$
$$\mathcal{R}\left(\widehat{r},\theta\right)_{x,z} = r_x r_z\left(1-\cos\theta\right) + r_y\sin\theta \tag{A7}$$
$$\mathcal{R}\left(\widehat{r},\theta\right)_{z,x} = r_z r_x\left(1-\cos\theta\right) - r_y\sin\theta \tag{A8}$$
$$\mathcal{R}\left(\widehat{r},\theta\right)_{y,z} = r_y r_z\left(1-\cos\theta\right) - r_x\sin\theta \tag{A9}$$
$$\mathcal{R}\left(\widehat{r},\theta\right)_{z,y} = r_z r_y\left(1-\cos\theta\right) + r_x\sin\theta \tag{A10}$$

for the off diagonal components. For the special case where $\vec{H}$ and $\widehat{u}$ are parallel, we assume that the magnetization is also parallel with $\widehat{u}$.

Acknowledgments

This work was supported by Natural Environment Research Council (UK) (Grant No.NE/S001018 and NE/S01197) to W.W., and NSF-NERC (Grant No. EAR1827263) to W.W. and L.T. Raw data used in this study is archived with DOI:10.5281/zenodo.5086636. The specific version of the code used to produce the data in this study is archived with DOI:10.5281/zenodo.5085691 and updated at `https://www.github.com/Lesleis-Nagy/sd-cooling`.

References

Biggin, A., Badejo, S., Hodgson, E., Muxworthy, A., Shaw, J., & Dekkers, M. (2013). The effect of cooling rate on the intensity of thermoremanent magnetization (trm) acquired by assemblages of pseudo-single domain, multidomain and interacting single-domain grains. *Geophys. J. Int.*, *193*(3), 1239–1249.

Bono, R. K., Tarduno, J. A., Nimmo, F., & Cottrell, R. D. (2019). Young inner core inferred from ediacaran ultra-low geomagnetic field intensity. *Nat. Geosci.*, *12*(2), 143–147.

Boost. (2021). *Boost C++ Libraries.* `http://www.boost.org/`. (Last accessed June 10 2020)

Cullity, B. D., & Graham, C. D. (2011). *Introduction to magnetic materials.* John Wiley & Sons.

Dodson, M. H., & McClelland-Brown, E. (1980). Magnetic blocking temperatures of single-domain grains during slow cooling. *J. Geophys. Res. B: Solid Earth*, *85*(B5), 2625–2637.

Driscoll, P. E. (2016). Simulating 2 ga of geodynamo history. *Geophys. Res. Lett.*, *43*(11), 5680–5687.

Dunlop, D. J., & Özdemir, Ö. (2001). *Rock magnetism: fundamentals and frontiers* (Vol. 3). Cambridge university press.

Fabian, K., & Shcherbakov, V. P. (2018). Energy barriers in three-dimensional micromagnetic models and the physics of thermoviscous magnetization. *Geophys. J. Int.*, *215*(1), 314–324.

Ferk, A., Aulock, F. v., Leonhardt, R., Hess, K.-U., & Dingwell, D. (2010). A cooling rate bias in paleointensity determination from volcanic glass: an experimental demonstration. *J. Geophys. Res. B: Solid Earth*, *115*(B8).

Fox, J., & Aitken, M. (1980). Cooling-rate dependence of thermoremanent magnetisation. *Nature*, *283*(5746), 462–463.

Guennebaud, G., Jacob, B., et al. (2010). *Eigen v3.* `http://eigen.tuxfamily.org`. (Last accessed June 10 2020)

Halgedahl, S., Day, R., & Fuller, M. (1980). The effect of cooling rate on the intensity of weak-field trm in single-domain magnetite. *J. Geophys. Res. B: Solid Earth*, *85*(B7), 3690–3698.

Leonhardt, R., Matzka, J., Nichols, A. R., & Dingwell, D. B. (2006). Cooling rate correction of paleointensity determination for volcanic glasses by relaxation geospeedometry. *Earth Planet. Sci. Lett.*, *243*(1-2), 282–292.

McClelland-Brown, E. (1984). Experiments on trm intensity dependence on cooling rate. *Geophys. Res. Lett.*, *11*(3), 205–208.

Néel, L. (1949). Théorie du trainage magnétique des ferromagneétiques en grains fines avec applications aux terres cuites. *Ann. Geophys.*, *5*, 99–136.

Ó Conbhuí, P., Williams, W., Fabian, K., Ridley, P., Nagy, L., & Muxworthy, A. R. (2018). Merrill: Micromagnetic earth related robust interpreted language laboratory. *Geochem. Geophys. Geosyst.*, *19*(4), 1080–1106.

Pozzo, M., Davies, C., Gubbins, D., & Alfè, D. (2012). Thermal and electrical conductivity of iron at earth's core conditions. *Nature*, *485*, 355-358.

Press, W. H., Teukolsky, S. A., Vetterling, W. T., & Flannery, B. P. (2007). *Numerical recipes: the art of scientific computing (3^{rd} ed.)*. Cambridge university press.

Santos, C. N., & Tauxe, L. (2019). Investigating the accuracy, precision, and cooling rate dependence of laboratory-acquired thermal remanences during paleointensity experiments. *Geochem. Geophys. Geosyst.*, *20*(1), 383–397.

Selkin, P., Gee, J., Tauxe, L., Meurer, W., & Newell, A. (2000). The effect of remanence anisotropy on paleointensity estimates: A case study from the archean stillwater complex. *Earth Planet. Sci. Lett.*, *182*, 403-416.

Stoner, E. C., & Wohlfarth, E. (1948). A mechanism of magnetic hysteresis in heterogeneous alloys. *Philos. Trans. R. Soc. London, Ser. A*, *240*(826), 599–642.

Tarduno, J. A., Cottrell, R. D., Bono, R. K., Oda, H., Davis, W. J., Fayek, M., ... Blackman, E. G. (2020). Paleomagnetism indicates that primary magnetite in zircon records a strong Hadean geodynamo. *Proceedings of the National Academy of Sciences*, *117*(5), 2309–2318. doi: 10.1073/pnas.1916553117

Tarduno, J. A., Cottrell, R. D., Watkeys, M. K., Hofmann, A., Doubrovine, P. V., Mamajek, E. E., ... Usui, Y. (2010). Geodynamo, solar wind, and magnetopause 3.4 to 3.45 billion years ago. *Science*, *327*(5970), 1238–1240.

Yu, Y. (2011). Importance of cooling rate dependence of thermoremanence in paleointensity determination. *J. Geophys. Res. B: Solid Earth*, *116*(B9).